Orbital physics of polar Fermi molecules

Omjyoti Dutta,[1] Tomasz Sowiński,[1,2] and Maciej Lewenstein[1,3]
[1]*ICFO—Institut de Ciencies Fotoniques, Av. Carl Friedrich Gauss, num. 3, 08860 Castelldefels (Barcelona), Spain*
[2]*Institute of Physics of the Polish Academy of Sciences, Al. Lotników 32/46, 02-668 Warsaw, Poland*
[3]*ICREA—Institució Catalana de Recerca i Estudis Avançats, Lluis Companys 23, E-08010 Barcelona, Spain*
(Received 24 April 2012; published 19 February 2013)

We study a system of polar fermions in a two-dimensional optical lattice and show that the multiband Fermi-Hubbard model is necessary to discuss its properties. We take into account both onsite and long-range interactions between different bands, as well as occupation-dependent inter- and intraband tunnelings. For strong-enough dipolar interactions we predict the appearances of phases such as multiband crystals, smectic metal, and exotic p-wave supersolids.

DOI: 10.1103/PhysRevA.87.023619 PACS number(s): 67.85.−d, 67.80.kb, 71.10.Fd

I. INTRODUCTION

Creation of ultracold heteronuclear molecules opens the path towards experimental realization of strongly interacting dipolar many-body systems. Depending on the constituent atoms, in moderate electric field these molecules can have a large dipole moment of 1 D in their vibrational ground states [1–4]. In particular, fermionic molecules in the presence of an optical lattice can be used to simulate various quantum phases, such as quantum magnetism and phases of t-J-like models [5–7], various charge density wave orders [8,9], bond-order solids [10], and so on. One should also stress that in the strongly correlated regime, in both bosonic and fermionic systems, the standard descriptions of single-band Hubbard model ceases to be valid. The effect of nonstandard terms become important, leading to novel phases like pair superfluidity and so on [11–16].

While most of the works have been dealing with higher bands concentrated on bosonic systems, in this paper, we study dipolar fermions confined in a 2D optical lattice $V_{\rm latt} = V_0[\sin^2(\pi x/a) + \sin^2(\pi y/a)] + \frac{m\Omega^2}{2}z^2$, where V_0 is the lattice depth, a is the lattice constant, m is the mass of the molecule, and Ω is the frequency of harmonic potential in the z direction. n is the fermion filling in the lattice. The dipoles are polarized along the direction of harmonic trapping. Usually, at low temperature and for low tunneling, the phase diagram consists of different crystal states whose structure depends on the filling n [8]. In this paper, we derive a Fermi-Hubbard model for dipolar fermions, including the effects of higher bands. We show that, even for moderate dipolar strength, it is necessary to take into account the excitations along the z direction. Simultaneously, in this regime, the interaction-induced hopping along the lattice is also important. This changes the phases expected for a so-called spinless Fermi-Hubbard model including only a single band. We want to point out that, as explained later, our model is not equivalent to the models with two distinguishable fermionic species.

Near $n \gtrsim 1/4$, we find a spontaneous appearance of non-Fermi liquid behavior in the form of smectic metallic phase. Near $n \gtrsim 1/2$, we find that the system can be mapped to an extended pseudo-spin-1/2 Hubbard model with a different emergent lattice configuration. We find a regime where chiral p-wave superconductivity emerges through a Kohn-Luttinger (KL) mechanism with a transition temperature T_c of the order of tunneling, the temperature where tunneling becomes likely. This gives rise to an exotic supersolid, with the diagonal long-range order provided by the checkerboard pattern of the lower orbital fermions, while the superfluidity originating from the fermions in the higher band.

The paper is organized as follows: In Sec. II we have introduced a multiorbital model to describe dipolar fermions in optical lattices. We then discuss quantitatively the contributions of different parameters present in the model. In Sec. III we have described the energy contribution of different crystal structures in the limit of vanishing tunneling. We also compare the corresponding energies of such crystal states without taking into account the higher bands and show that it is necessary to take into account the higher band contributions for experimentally realizable parameters. In Sec. IV, we have investigated the ground-state properties for filling greater than 1/4. We find that due to the higher band-occupation-dependent tunneling contributions, within a certain parameter regime, there is a spontaneous formation of the smectic-metal phase, along with stripelike phases. In Sec. V we describe the ground-state structures for $n \gtrsim 1/2$. We find that the higher-band tunneling can give rise to sublattices which further can give rise to p-wave superfluidity. In Sec. VI we present our conclusions followed by acknowledgments in Sec. VII.

II. MODEL

The Hamiltonian for the dipolar fermions in the second quantized form reads

$$H = \int d^3\boldsymbol{r}\Psi^\dagger(\boldsymbol{r})H_0\Psi(\boldsymbol{r}) + \frac{1}{2}\int d^3\boldsymbol{r}\, d^3\boldsymbol{r}'\Psi^\dagger(\boldsymbol{r})\Psi^\dagger(\boldsymbol{r}')\mathcal{V}(\boldsymbol{r}-\boldsymbol{r}')\Psi(\boldsymbol{r}')\Psi(\boldsymbol{r}), \quad (1)$$

where $\Psi(\boldsymbol{r})$ is a spinless fermion field operator satisfying anticommutation relations $\{\Psi(\boldsymbol{r}),\Psi^\dagger(\boldsymbol{r}')\} = \delta(\boldsymbol{r}-\boldsymbol{r}')$ and $\{\Psi(\boldsymbol{r}),\Psi(\boldsymbol{r}')\} = 0$. In the units of recoil energy $E_R = \pi^2\hbar^2/(2ma^2)$, the lattice confinement in the z direction is characterized by the dimensionless parameter $\kappa = \hbar\Omega/(2E_R)$, and the single-particle Hamiltonian becomes $H_0 = -\nabla^2 + V_{\rm latt}(\boldsymbol{r})/E_R$. The long-range interaction potential reads $\mathcal{V}(\boldsymbol{r}) = D(1/r^3 - 3z^2/r^5)$, where $D = 2\pi md^2/(\hbar^2 a)$ is a dimensionless dipolar strength, related to the electric dipolar moment

d. For KRb molecules with a dipole moment of 0.5 D confined in the optical lattice with $a = 345$ nm [17] one gets $D = 8.6$, whereas, for similar lattice parameters, LiCs molecules can have a dipole moment of ∼5 D with $D \sim 100$. We decompose the field operator in the basis of Wannier functions in the x and y directions and of harmonic oscillator eigenstates in the z direction. For convenience, we introduce the orbital index $\sigma = \{pml\}$ denoting p, m, and l excitations in the x, y, and z directions, respectively. In this basis the field operator $\Psi(\boldsymbol{r}) = \sum_{i,\sigma} \hat{a}_{i\sigma} \mathcal{W}_{i\sigma}(\boldsymbol{r})$, where $\mathcal{W}_{i\sigma}(\boldsymbol{r})$ is the single-particle wave function in orbital σ localized on site $\boldsymbol{i} = i_x \boldsymbol{e}_x + i_y \boldsymbol{e}_y$ ($\boldsymbol{e}_x$ and $\boldsymbol{e}_y$ are unit vectors in the proper directions). Fermionic operator $\hat{a}_{i\sigma}$ annihilates particle in this state. They satisfy fermionic anticommutation relations, $\{\hat{a}_{i\sigma}, \hat{a}^\dagger_{j\sigma'}\} = \delta_{\sigma,\sigma'}\delta_{ij}$. The Hamiltonian can be rewritten in the following Hubbard-like form $H = \sum_\sigma \mathcal{H}^{(1)}_\sigma + \sum_{\sigma\sigma'} \mathcal{H}^{(2)}_{\sigma\sigma'}$, where

$$\mathcal{H}^{(1)}_\sigma = E_\sigma \sum_{\boldsymbol{i}} \hat{n}_{i\sigma} + J_\sigma \sum_{\{\boldsymbol{ij}\}} \hat{a}^\dagger_{i\sigma} \hat{a}_{j\sigma}, \tag{2a}$$

$$\mathcal{H}^{(2)}_{\sigma\sigma'} = U_{\sigma\sigma'} \sum_{\boldsymbol{i}} \hat{n}_{i\sigma}\hat{n}_{i\sigma'} + \sum_{\boldsymbol{i}\neq\boldsymbol{j}} V_{\sigma\sigma'}(\boldsymbol{i}-\boldsymbol{j})\hat{n}_{i\sigma}\hat{n}_{j\sigma'} + \sum_{\{\boldsymbol{ij}\}} \sum_{\sigma''} T^{\sigma''}_{\sigma\sigma'}(\boldsymbol{i}-\boldsymbol{j})\hat{a}^\dagger_{i\sigma}\hat{n}_{i\sigma''}\hat{a}_{j\sigma'}. \tag{2b}$$

Parameters E_σ and J_σ come from the single-particle Hamiltonian and denote single-particle energy and nearest-neighbor tunneling in orbital σ, respectively. The interparticle interaction has three contributions to the Hamiltonian (2b) as follows: (i) the onsite interaction energy of fermions occupying different orbitals σ and σ' of the same site $U_{\sigma\sigma'}$, (ii) the long-range interaction energy of fermions occupying orbitals σ and σ' of different sites $V_{\sigma\sigma'}(\boldsymbol{i}-\boldsymbol{j})$, and (iii) the tunneling from orbital σ' at site $\boldsymbol{j}$ to the orbital σ at site $\boldsymbol{i}$ induced by the presence of an additional fermion at site $\boldsymbol{i}$ in orbital σ'' denoted by $T^{\sigma''}_{\sigma\sigma'}(\boldsymbol{i}-\boldsymbol{j})$. Without the loss of generality we can set $E_s = 0$.

The Hamiltonian (2) is very general. To get a physical understanding of its properties, we start by examining the properties of density-density interactions. We calculate the interactions between a few of the lowest bands: $s = \{000\}$, $p_x = \{100\}$, $p_y = \{010\}$, $p_z = \{001\}$, $p_{xz} = \{101\}$, and $p_{yz} = \{011\}$. We find that the onsite interactions $U_{s,p_x} = U_{s,p_y}$ are always repulsive. This means that putting two fermions in s and p_x or p_y orbitals simultaneously is energetically unfavorable. Remarkably, we find that U_{s,p_z} is always negative. This surprising attraction stems from the presence of the fermionic exchange term and the shape of the dipolar interactions (see Appendix A). The negativity of U_{s,p_z} cannot be solely explained by the attractive nature of the dipolar interaction separated along the z direction. It comes from the fact that the indistinguishable fermions occupy two orbitals in the same site. Therefore, it is not present in models with two different species as well as dipolar bosons. For higher orbitals, we find that $|U_{s,p_z}| \gg |U_{s,p_{xz}}| = |U_{s,p_{yz}}|$. As U_{s,p_z} is negative, we look into the κ-D parameter space to investigate the breakdown of single-band approximation since two particles can occupy the same site. This behavior is controlled by the onsite energy cost $\Delta = E_z + U_{s,p_z}$, where the energy gap between the s and p_z orbitals is given by $E_z = \hbar\Omega$. In Fig. 1(a), for a fixed dipolar strength $D = 8$, we see that Δ becomes negative when the lattice confinement κ goes below some critical value. In Fig. 1(b), we plot Δ as a function of dipolar strength D and we see that, above some critical dipolar strength D, Δ becomes negative. This value of the critical D also decreases as the lattice confinement κ goes down. This also suggests that for low κ, the single-band approximation will break down even for lower dipolar strength D. In Fig. 2(a), we plot the various interaction strengths among different bands as a function of lattice confinement κ. We note that, in addition for long-range interactions, we find that $V_{s,s}(\boldsymbol{i}) > V_{s,p_z}(\boldsymbol{i}) > V_{p_z,p_z}(\boldsymbol{i}) > 0$. This results in the breaking of the single-band approximation due to presence of the p_z orbital. Thus, it is important to take into account at least the s and p_z orbitals to describe the dipolar fermions.

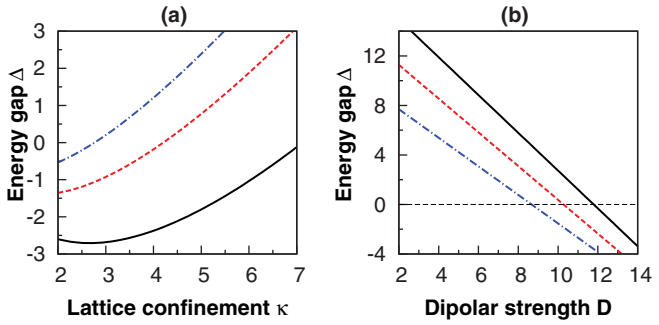

FIG. 1. (Color online) (a) We plot Δ as a function of lattice confinement κ for different values of lattice depth V_0 and dipolar strength $D = 8$. The black solid line, red dashed line, and blue dash-dotted lines correspond to $V_0 = 12E_R$, $8E_R$, and $6E_R$, respectively. (b) Here we plot Δ as a function of dipolar strength D for different values of lattice confinement κ and lattice depth $V_0 = 8E_R$. The black solid line, red dashed line, and blue dash-dotted lines correspond to $\kappa = 9$, 7, and 5, respectively.

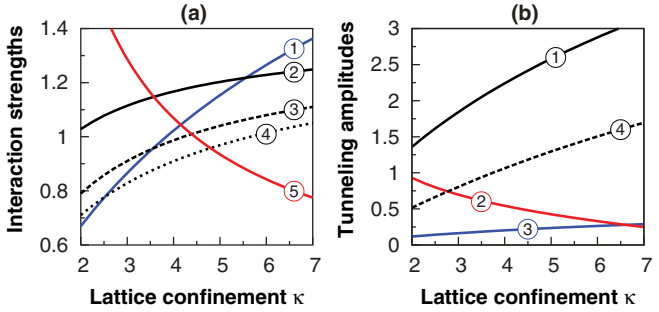

FIG. 2. (Color online) Parameters of the Hamiltonian for $V_0 = 8E_R$ as functions of the lattice confinement κ. (a) Onsite interaction $-\frac{U_{s,p_z}}{DE_R}$ (blue solid line, -1-) and nearest-neighbor long-range interactions $\frac{V_{s,s}(\boldsymbol{e}_x)}{DJ_s}$ (solid black line, -2-), $\frac{V_{s,p_z}(\boldsymbol{e}_x)}{DJ_s}$ (dashed black line, -3-), and $\frac{V_{p_z,p_z}(\boldsymbol{e}_x)}{DJ_s}$ (dotted black line, -4-). The red line (-5-) shows the ratio $V_{p_z,p_z}(2\boldsymbol{e}_x)/T^{\parallel}_{\text{eff}}$. (b) Magnitudes of the induced tunneling terms $\frac{T^s_{p_z,p_{xz}}(\boldsymbol{e}_x)}{DJ_s}$ (black solid line, -1-), $\frac{T^s_{s,p_x}(\boldsymbol{e}_x)}{DJ_s}$ (red solid line, -2-), and $\frac{T^s_{p_z,p_z}(\boldsymbol{e}_x)}{DJ_s}$ (blue solid line, -3-). The dashed black line (-4-) denotes the ratio $T^{\parallel}_{\text{eff}}/J_s$ for $D = 10$.

We next discuss the role of the interaction-induced tunnelings in Hamiltonian (2). Counterintuitively the most important contribution does not come from the induced tunneling in the p_z band ($T^s_{p_z,p_z}(\boldsymbol{e}_x)$) but from the interband tunneling which changes the p_z orbital to the p_{xz} and p_{yz} ones ($T^s_{p_z,p_{xz}}(\boldsymbol{e}_x)$). Note that this interband tunneling is absent for usual single-particle tunneling as the Wannier states of different orbitals belongs to different Bloch bands [18]. From properties of p orbital states it follows that $T^s_{p_z,p_{xz}}(-\boldsymbol{e}_x) = -T^s_{p_z,p_{xz}}(\boldsymbol{e}_x)$. The relation of this term to other interaction-induced tunnelings is shown in Fig. 2(b). From the above analysis we introduce a simplified, but realistic, model of polar Fermi molecules confined in a 2D optical lattice by taking into account effects of interactions between orbitals $\sigma \in \{s, p_z, p_{xz}, p_{yz}\}$. As we show later, the effect of $\{p_{xz}, p_{yz}\}$ orbitals can result in strong long-range tunneling which is absent in the usual tight-binding models. Thus, the effect of orbitals higher in energy can, additionally, give rise to new processes which cannot be taken into account by renormalization of the parameters.

At this point let us note that our model shines a light on the various spin-Hamiltonian simulators created via polar molecules in optical lattices [5–7]. The standard way of treating such a systems is to rewrite a Hamiltonian as an effective spin model under the assumption that each lattice site can be occupied at most by one molecule. This simply means that one neglects the interaction between two indistinguishable particles at the same site. From our analysis, it follows that this assumption definitely breaks down when $\Delta = E_z + U_{s,p_z} < 0$, which is controlled by the dipolar strength D, optical lattice depth V_0, and trapping frequency Ω, as plotted in Figs. 1(a) and 1(b). As one increases the lattice depth or dipolar strength, the trapping frequency in the z direction Ω must be increased to prevent the breaking of the single-band approximation. This observation limits the parameter regimes accessible for the models used in Refs. [5–7].

III. CLASSICAL GROUND STATE OF THE SYSTEM

To find the ground state of the system for a given filling, we first look for the classical crystal states in the limit of vanishing tunneling. Such an approach is valid as long as the excitation energies of the crystal state are much larger than the tunneling. To find the lowest-energy classical crystal states we follow the strategy described in Refs. [19,20]. Without the higher orbital effects, at most one fermion can occupy a given site. The corresponding Hamiltonian reads

$$\mathcal{H}_I = \sum_{\boldsymbol{i}\neq\boldsymbol{j}} V_{ss}(\boldsymbol{i}-\boldsymbol{j})\hat{n}_{\boldsymbol{i}s}\hat{n}_{\boldsymbol{j}s} \tag{3}$$

with the dipolar interaction in the s band $V_{ss}(\boldsymbol{i}-\boldsymbol{j}) = V_{ss}/|\boldsymbol{i}-\boldsymbol{j}|^3$.

By taking the orbital effects into account, the corresponding Hamiltonian is defined in Eq. (2),

$$\mathcal{H}_{\rm II} = E_\sigma \sum_{\boldsymbol{i}} \hat{n}_{\boldsymbol{i}\sigma} + \sum_{\sigma} U_{\sigma\sigma'} \sum_{\boldsymbol{i}} \hat{n}_{\boldsymbol{i}\sigma}\hat{n}_{\boldsymbol{i}\sigma'} + \sum_{\sigma,\sigma'}\sum_{\boldsymbol{i}\neq\boldsymbol{j}} V_{\sigma\sigma'}(\boldsymbol{i}-\boldsymbol{j})\hat{n}_{\boldsymbol{i}\sigma}\hat{n}_{\boldsymbol{j}\sigma}, \tag{4}$$

where σ denotes the s and p_z orbital fermions.

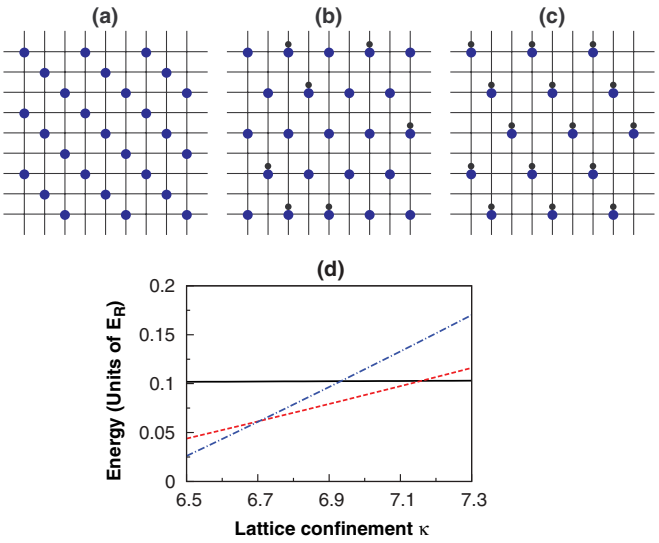

FIG. 3. (Color online) Pictorial diagram of the different checkerboard lattices for $n = 1/3$. The blue spheres denote s-orbital fermions and the smaller black spheres denote p_z orbital fermions. (a) Ground-state crystal phase of Hamiltonian (3). (b) A 1/4 checkerboard lattice of s-band fermions and extra p_z fermions with density 1/12. (c) Density-wave structure of the effective bosons with filling $n^b = 1/6$ corresponding to the ground-state structure of the Hamiltonian (5). (d) The energies E_{3A} (thick solid line), E_{3B} (dashed line), and E_{2C} (thin solid line) as functions of the trap frequency $\hbar\Omega/2E_R$ for dipolar strength $D = 10$.

We now consider the situation where each occupied site contains two fermions. In this case, we can define a corresponding hard-core bosonic operator at site $\boldsymbol{i}$ as $\hat{b}^\dagger_{\boldsymbol{i}} = s^\dagger_{\boldsymbol{i}} p^\dagger_{z\boldsymbol{i}}$ and $\hat{b}_{\boldsymbol{i}} = p_{z\boldsymbol{i}} s_{\boldsymbol{i}}$ and the bosonic number operator $\hat{n}^b_{\boldsymbol{i}} = \hat{b}^\dagger_{\boldsymbol{i}}\hat{b}_{\boldsymbol{i}}$. Subsequently, we can write an effective bosonic Hamiltonian as

$$\mathcal{H}_{\rm III} = \Delta \sum_{\boldsymbol{i}} \hat{n}^b_{\boldsymbol{i}} + \sum_{\boldsymbol{i}\neq\boldsymbol{j}}\sum_{\sigma,\sigma'} V_{\sigma\sigma'}(\boldsymbol{i}-\boldsymbol{j})\hat{n}^b_{\boldsymbol{i}}\hat{n}^b_{\boldsymbol{j}}, \tag{5}$$

where $\sigma,\sigma' = s, p_z$ and Δ is the energy cost of having a composite boson as defined before. Equation (5) is similar to the bosonic dipolar system with a modified dipolar interaction and can simulate the crystal phases of dipolar bosons [21].

For concreteness, we first specifically choose $n = 1/3$. At filling $n = 1/3$ the ground state of the single-band Hamiltonian (3) forms a crystal structure in accordance with Ref. [8] and it is shown in Fig. 3(a). Its energy is E_{3a}. In the current paper, we analyze other structures as a ground states corresponding to the full Hamiltonian (4) from general arguments given in Refs. [19,20]. Two other structures can form the lowest-energy states and are presented in Figs. 3(b) and 3(c) with corresponding energies E_{3b} and E_{3c}. In the $3b$ structure the s-band fermions form a 1/4 crystal structure and the remaining 1/12 p-orbital fermions occupy already-occupied sites. The third possible ground-state candidate Fig. 3(c) comes from the effective bosonic Hamiltonian (5) at filling $n_b = 1/6$. The energies of the three structures are plotted as functions of the harmonic trapping frequency for a dipolar strength $D = 10$ [Fig. 3(d)]. We find that the energy of the structure $3a$ is almost insensitive to the trapping frequency

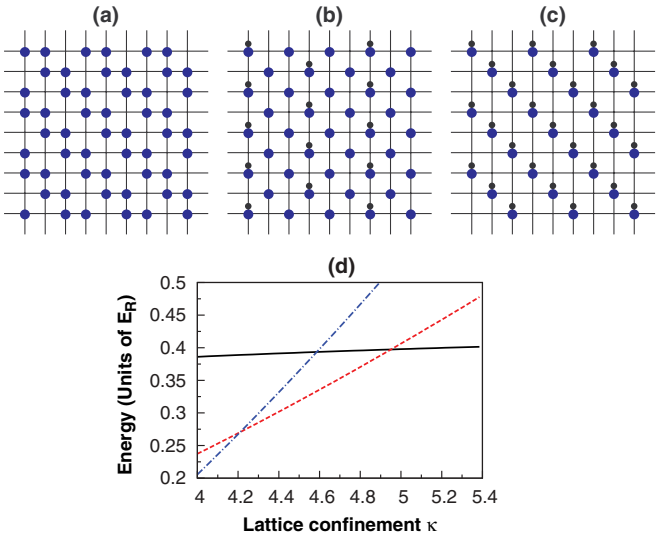

FIG. 4. (Color online) Pictorial diagram of the different checkerboard lattices for $n = 2/3$. The blue spheres denote s-orbital fermions and the smaller black spheres denote p_z orbital fermions. (a) Ground-state crystal phase of Hamiltonian (3). (b) A 1/2 checkerboard lattice of s-band fermions and extra p_z fermions with density 1/6. (c) Density-wave structure of the composite bosons with filling $n^b = 1/3$ corresponding to the ground-state structure of the Hamiltonian (5). (d) The energies E_{3A} (thick solid line), E_{3B} (dashed line), and E_{3C} (thin solid line) as functions of the trap frequency $\hbar\Omega/2E_R$ for dipolar strength $D = 8$.

Ω. Moreover, the structure is the lowest-energy state (the true ground state of the system) only for large-enough Ω ($\hbar\Omega \gtrsim 14.5E_R$ for studied case). For lower trap frequencies we find that structure $3b$ ($13.2E_R \lesssim \hbar\Omega \lesssim 14.5E_R$) or $2c$ ($\hbar\Omega \lesssim 13.2E_R$) becomes a ground state of the system. We have also checked that, for filling factors between $n = 1/4$ and $n = 1/3$, the energy of the configuration $3b$ is lower than the energy of the phase-separated structures predicted for single-band models [8].

Similarly, we also can infer the ground-state structures at filling $n = 2/3$ as the situation is very similar to the filling $n = 1/3$ due to particle-hole symmetry. The ground state of the single-band Hamiltonian (3) shown in Fig. 4(a) with corresponding energy E_{4a} is a true ground state of the system only for large-enough Ω. For lower confinement κ the ground state is (i) a 1/2 checkerboard s-band crystal with p-band fermions (with density 1/6) moving on the occupied sites [energy E_{4b} and Fig. 4(b)] or (ii) a $n_b = 1/3$ stripe structure of composite bosons [energy E_{4c} and Fig. 4(c)] [21]. Similar results are also obtained for other filling fractions, namely $n = 1/4, 1/2, 3/4$. For these filling fractions we also find that below a certain critical trapping strength Ω, for critical D, it is important to take into account the excited trap states.

We next discuss the effect of s-fermion tunneling on the ground-state structures obtained for 1/3 filling. For the 1/3 crystal in Fig. 3(a), s-orbital tunneling can displace a molecule from their classical state with excitation energy $\sim 1.7V_s s \ll J_s$ for $D = 10$. Thus, such excitations will be localized and will not melt the 1/3 crystal. Similarly for the structure in Fig. 3(a), the s-orbital fermions for a 1/4 crystal with the corresponding excitation energy is given by $\sim 0.3V_{ss} \ll J_s$ for $D = 10$. Therefore, such states are stable with respect to s-orbital tunneling. We also note that for the structure $3c$, within the bosonic subspace, tunneling can arise in second-order processes and it is much lower than the binding energy of the bosons. The stability of structures like $3b$ with respect to p_z-orbital fermions will be discussed in the following sections.

IV. GROUND-STATE STRUCTURES NEAR $n \gtrsim 1/4$

In this section we will look into the properties of the ground states near $n = 1/4$ filling. We show that the presence of higher orbitals not only changes the ground-state crystal structures, it also fundamentally changes the properties of such states. Specifically, we show that new forms of matter, like the smectic metal phase, can spontaneously form due to the effect of higher orbitals.

Here we consider the case when $\Delta > 0$ and, therefore, for low filling all fermions occupy only the s-orbital states. For filling $n = 1/4$ and large-enough D ($\gtrsim 3$) there is a nonvanishing single-particle excitation gap and the system is in the s-band insulator state [denoted by blue spheres in Fig. 5(a)] [8]. Situation changes dramatically for higher fillings. It can be simply understood using energy arguments.

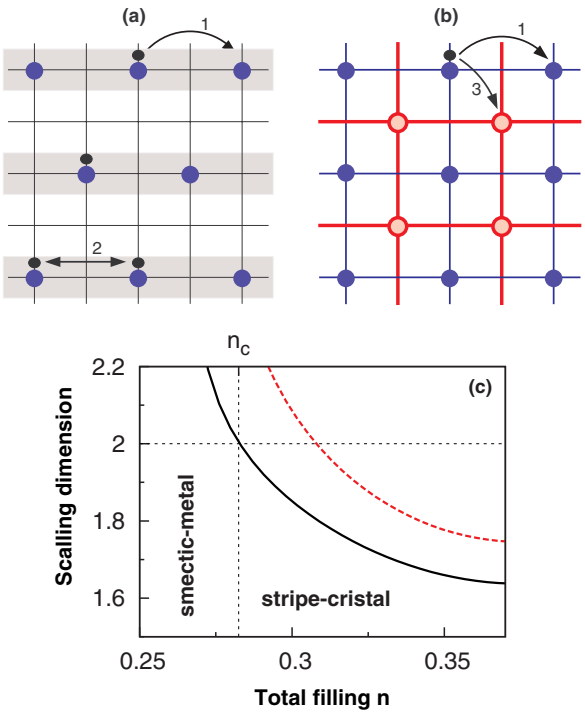

FIG. 5. (Color online) Pictorial diagram of the different checkerboard lattices. The solid blue and open red spheres denotes s-orbital fermions and the smaller black sphere denotes p_z orbital fermions. (a) Checkerboard lattice at $n = 1/4$ filling. The p_z fermions will move with effective tunneling $T_{\text{eff}}^{\parallel}$ (arrow 1) only along the shaded region, making a stack of 1D chains. Interaction between neighboring p-band fermions is equal to $V_{p_z,p_z}(2\boldsymbol{e}_x)$ (arrow 2). (b) Scaling dimensions η_1 (solid line) and η_2 (dashed line) as functions of the total density n for $D = 10$ and $\hbar\Omega = 14E_R$. (c) Checkerboard lattice at $n = 1/2$. The blue and thick red lines constitute two different sublattices. They are not coupled via tunneling processes since the tunneling $T_{\text{eff}}^{\perp}$ (arrow 3) is much smaller than $T_{\text{eff}}^{\parallel}$.

The energy cost of putting additional particles in the vacant site is given by $E_{\rm vac} = V_{s,s}(\boldsymbol{e}_x) + 2V_{s,s}(\boldsymbol{e}_x + \boldsymbol{e}_y) + \cdots$. In contrast, the cost of putting additional particles to the p_z orbital of an occupied site is $E_{\rm occ} = \Delta + 2V_{s,p_z}(2\boldsymbol{e}_x) + \cdots$. For D larger than some critical strength one finds that $E_{\rm occ} < E_{\rm vac}$. As an example, such conditions are fulfilled for $V_0 = 8E_R$, $D = 10$, and $\hbar\Omega \leqslant 14E_R$. Consequently, additional particles start to fill the p_z band of previously occupied sites. In this scenario, energy-conserving dynamics of the system comes from the second-order processes involving tunneling to the next occupied site [along the x direction in Fig. 5(a)]. To the leading order, this effective tunneling is given by

$$T^{\parallel}_{\rm eff} \approx T^{s}_{s,p_z}(\boldsymbol{e}_x)^2 \big/ (|U_{s,p_z}| + E_x). \tag{6}$$

As p_z fermions only exist with another s fermion in the same site, the p_z fermions can tunnel (with $T^{\parallel}_{\rm eff}$) along one direction chosen by the insulator checkerboard geometry in s band, in our case along $\boldsymbol{e}_x$ [Fig. 5(a)]. Along $\boldsymbol{e}_y$, on the other hand, there is no s-orbital fermion where a p_z fermion can hop directly or by use of a second-order process without going to an higher energy state. Thus, the movement of the p_z fermions is confined only to along $\boldsymbol{e}_x$. Thus, the resulting system can be thought as stacks of one-dimensional chains or stripes placed along $\boldsymbol{e}_y$ without interchain tunnelings [22]. The effective Hamiltonian governing the p_z fermions can be written as $H_{\rm 1D} = T^{\parallel}_{\rm eff}\sum_l \sum_{\langle ij\rangle} \hat{c}^{\dagger}_{l,i}\hat{c}_{l,j} + H_{\rm intra} + H_{\rm inter}$ with intrachain Hamiltonian $H_{\rm intra} = \sum_l \sum_{i,j} V_{\rm intra}(i,j)\hat{c}^{\dagger}_{l,i}\hat{c}_{l,i}\hat{c}^{\dagger}_{l,j}\hat{c}_{l,j}$ and interchain Hamiltonian $H_{\rm inter} = \sum_{l,l'}\sum_{i,i'} V_{l,l'}(i,i')\hat{c}^{\dagger}_{l,i}\hat{c}_{l,i}\hat{c}^{\dagger}_{l',i'}\hat{c}_{l',i'}$, where $\hat{c}^{\dagger}_{l,i_x}$ and $\hat{c}_{l,i_x}$ are creation and annihilation operators of p_z fermions on the s-fermion-occupied site i on chain l. The intrachain and interchain interactions are given by $V_{\rm intra}(i,j) = V_{p_z,p_z}([i-j]\boldsymbol{e}_x)$ and $V_{l,l'}(i,i') = V_{p_z,p_z}([i-i']\boldsymbol{e}_x + [l-l']\boldsymbol{e}_y)$, respectively.

The ground-state structure of this coupled-chain system is investigated by introducing the bosonized fields $\phi_{l,R/L}$ related to the Fermi operator $\hat{c}_{l,i}$ rewritten in the continuum limit as $\hat{c}_{l,i} \to \Psi_{l,L}(x) + \Psi_{l,R}(x)$ [23,24]. Near the left and right Fermi momenta $\pm\tilde{k}_1$, we can write $\Psi_{l,R/L}(x) = F_{R/L}\exp[\pm i\tilde{k}_1 x - i\phi_{l,R/L}(x)]/\sqrt{2\pi\epsilon}$, where ϵ is a cutoff length and $F_{R/L}$ are Klein factors. The Fermi momentum is given by the density of p_z fermions which, in terms of total density n, reads $\tilde{k}_1 \approx (4n-1)\pi$. By writing the bosonized phase field $\theta_l(x) = [\phi_{l,L}(x) - \phi_{l,R}(x)]/2\sqrt{\pi}$ in terms of its Fourier transform $\theta_{q_y}(x)$ along $\boldsymbol{e}_y$, the Lagrangian for the system reads

$$\mathcal{L} = \int_{-\pi}^{\pi}\frac{dq_y}{2\pi}\frac{K(q_y)}{2}\left[\frac{1}{v(q_y)}\left(\frac{\partial\theta_{q_y}}{\partial t}\right)^2 - v(q_y)\left(\frac{\partial\theta_{q_y}}{\partial x}\right)^2\right]. \tag{7}$$

The interaction parameter $K(q_y)$ and sound velocity $v(q_y)$ are determined by the details of the dipolar interactions (see Appendix C).

Interchain interactions induce additional charge-density wave (CDW) perturbation, $\mathcal{L}_{\rm CDW} = \mathcal{L}_{\rm CDW,1} + \mathcal{L}_{\rm CDW,2} + \cdots$, with

$$\mathcal{L}_{\rm CDW,1} = \frac{1}{u}\sum_N V_{p_z,p_z}((2N+1)\boldsymbol{e}_x + 2\boldsymbol{e}_y)\cos[(2N+1)\tilde{k}_1] \times \sum_l \cos[2\sqrt{\pi}(\theta_l - \theta_{l+1})], \tag{8a}$$

$$\mathcal{L}_{\rm CDW,2} = \frac{1}{u}\sum_N V_{p_z,p_z}(2N\boldsymbol{e}_x + 4\boldsymbol{e}_y)\cos[(2N)\tilde{k}_1] \times \sum_l \cos[2\sqrt{\pi}(\theta_l - \theta_{l+2})]. \tag{8b}$$

Here $\mathcal{L}_{\rm CDW,L}$ is the CDW coupling between two chains with distance $L = 1,2,\ldots$. Consequently, following Ref. [25], the scaling dimension of the CDW operator is given by $\eta_L = 2\int_{-\pi}^{\pi}\frac{1-\cos Lq_y}{K(q_y)}\frac{dq_y}{2\pi}$. When $\eta_L > 2$ for all L, the CDW operator is irrelevant. The stable phase then has properties similar to a 1D Luttinger liquid with low-energy bosonic collective excitations. This state preserves the smectic symmetry $\theta_l \to \theta_l + \alpha_l$, with α_l constant on each chain. This phase is known as the *smectic-metal* phase [23] as there is metallic behavior along the chain with an insulating density wave order along the transverse direction. This phase is a peculiar example of the spontaneous emergence of non-Fermi liquid behavior in two-dimensional Fermi systems. In contrast, when $\eta_L < 2$, then p_z fermions becomes unstable towards formation of stripe crystals. In Fig. 5(b) we plot η_1 and η_2 as functions of total density n for $D = 10$ and $\hbar\Omega = 14E_R$. It is clear that for $1/4 < n < n_c$ there is a *smectic-metallic* phase while, for $n > n_c$, the system goes to a stripe-crystal phase. We have checked η_L to $L = 4$ and all reside between η_1 and η_2.

V. GROUND-STATE STRUCTURES NEAR $n \gtrsim 1/2$

In this section let us discuss the case of filling $n = 1/2$ where, for low dipolar strength D, due to the same reasons as before, fermions will occupy only the s band and the ground state of the system is the checkerboard insulator (see Appendix C), as denoted by the solid blue and open red spheres in Fig. 5(b). To look for properties of the system with additional particles, we define the deviation from half-filling $\delta n = n - 1/2$ and we introduce the corresponding chemical potential $\mu(\delta n)$. From energy arguments we find that two scenarios can occur. The additional fermion (i) occupies a vacant site with energy cost $E_{\rm vac} = 4V_{s,s}(\boldsymbol{e}_x) + 8V_{s,s}(2\boldsymbol{e}_x + \boldsymbol{e}_y) + \cdots$ or (ii) it goes to the p_z orbital of an occupied site with energy cost $E_{\rm occ} = \Delta + 4V_{s,p_z}(\boldsymbol{e}_x + \boldsymbol{e}_y) + V_{s,p_z}(2\boldsymbol{e}_x) + \cdots$. Consequently, in the second scenario (when $E_{\rm occ} \leqslant E_{\rm vac}$), all extra fermions will occupy the p_z orbitals of the already occupied sites. As an example, such conditions are fulfilled for $V_0 = 8E_R$, $D = 8$, and $\hbar\Omega \leqslant 10E_R$. In such a case, δn corresponds to the filling of p_z band fermions. The parallel tunneling of the p_z fermions between the occupied sites will again arise from the second-order processes (6). Moreover, tunneling to the diagonally occupied site $T^{\perp}_{\rm eff} \approx -[J_s - T^{s}_{p_z,p_z}(\boldsymbol{e}_x)]^2/|U_{s,p_z}|$, for $D \sim 8$ it is 400 times smaller than $T^{\parallel}_{\rm eff}$. Consequently, fermions in the p_z orbitals can move in independent square sublattices [either the thick red or blue sublattice shown in the Fig. 5(b)]. Note that fermions cannot tunnel between different sublattices. Thus, we can

describe the system of the p_z fermions in the blue (thick red) lattice as pseudo-spin-up (-down). By introducing operators $\hat{c}_{is}$, where $s \in \{\uparrow,\downarrow\}$, the effective Hamiltonian can be written as $H_{\rm eff} = T^{\parallel}_{\rm eff}\sum_s \sum_{\{ij\}} \hat{c}^{\dagger}_{is}\hat{c}_{js} + H_{\rm int}$ with

$$H_{\rm int} = V_{\uparrow\uparrow}\sum_s \sum_{\{ij\}} \hat{n}_{is}\hat{n}_{js} + V_{\uparrow\downarrow}\sum_{[ij]} \hat{n}_{i\uparrow}\hat{n}_{j\downarrow}, \tag{9}$$

where $\hat{n}_{is} = \hat{c}^{\dagger}_{is}\hat{c}_{is}$. For convenience we introduce $V_{\uparrow\uparrow} = V_{p_z,p_z}(2\boldsymbol{e}_x)$ and $V_{\uparrow\downarrow} = V_{p_z,p_z}(\boldsymbol{e}_x + \boldsymbol{e}_y)$. Note that now $\{.\}$ is understood as a nearest-neighbor in a given sublattice. Nearest neighbors between different sublattices is denoted by $[.]$. The modified lattice constant of the sublattices is $\widetilde{a} = 2a$. In this way we are able to study the system properties with the weak-coupling theory. We investigate the emergence of triplet superconductivity between the same pseudospin fermions, arising via the KL mechanism [18] (magnetic instabilities are discussed in Appendix D). We look for Cooper pairs with chiral p-wave symmetry. The effective interaction between fermions in KL mechanism in terms of the scattering momentum $\mathbf{k} - \mathbf{k}' = \mathbf{q}$ can be written as

$$V_{{\rm eff}\ s,s}(\boldsymbol{q}) = V_{\uparrow\uparrow}\eta_{\boldsymbol{q}} - \sum_{\boldsymbol{p}}\big[\big(V^2_{\uparrow\uparrow}\,\eta^2_{\boldsymbol{q}} + V^2_{\uparrow\downarrow}\,\beta^2_{\boldsymbol{q}}\big)Q_{\boldsymbol{q},\boldsymbol{p}} - 2V^2_{\uparrow\uparrow}\eta_{\boldsymbol{q}}\eta_{\boldsymbol{k}-\boldsymbol{p}}Q_{\boldsymbol{q},\boldsymbol{p}} - V^2_{\uparrow\uparrow}\eta_{\boldsymbol{k}'-\boldsymbol{p}}\eta_{\boldsymbol{k}-\boldsymbol{p}}Q_{\boldsymbol{k}+\boldsymbol{k}',\boldsymbol{p}}\big], \tag{10}$$

where $Q_{\boldsymbol{q},\boldsymbol{p}} = \frac{f(\epsilon_{\boldsymbol{p}})-f(\epsilon_{\boldsymbol{p}-\boldsymbol{q}})}{\epsilon_{\boldsymbol{p}-\boldsymbol{q}}-\epsilon_{\boldsymbol{p}}}$, $f(\epsilon)$ is the Fermi distribution function, $\epsilon_{\boldsymbol{p}} = 2T^{\parallel}_{\rm eff}[\cos(q_x\widetilde{a}) + \cos(q_y\widetilde{a})]$ is the dispersion and $\eta_{\boldsymbol{q}} = 2[\cos(q_x\widetilde{a}) + \cos(q_y\widetilde{a})]$ and $\beta_{\boldsymbol{q}} = 4[\cos(q_x\widetilde{a}/2)\cos(q_y\widetilde{a}/2)]$. The summation in (10) comes from taking into account the second-order terms represented by diagrams shown in Fig. 6(a). The two terms inside the first bracket in (10) comes from the top-left diagram in Fig. 6(a), while the next two terms comes from the top-right and bottom-left diagrams representing vertex corrections. The last term in (10) comes from the bottom-right diagram in Fig. 6(a) denoting exchange interactions. By performing the integration over the momentum in the limit of $T \to 0$, we finally get antisymmetric part of effective coupling $\{V_{\rm eff}(\boldsymbol{q})\}_- = -\lambda(T,\mu)[\sin(k_x\widetilde{a})\sin(k'_x\widetilde{a}) + \sin(k_y\widetilde{a})\sin(k'_y\widetilde{a})]$, where $\lambda(T,\mu) = 2V_{\uparrow\uparrow} + \frac{V^2_{\uparrow\uparrow}}{\pi T^{\parallel}_{\rm eff}}F_1(T,\mu) - \frac{V^2_{\uparrow\downarrow}}{\pi T^{\parallel}_{\rm eff}}F_2(T,\mu)$. Functions F_1 and F_2 originate in the second-order corrections and their detailed forms are given in Appendix E. The point is that, due to the Van Hove singularity in density of states, function F_2 contains a logarithmic divergence. At the same time, function F_1 is analytical due to the dressing of the density of states. This means that there always exists a finite critical μ above which the interaction is attractive and superfluidity appears. From the BCS theory one can get an estimate of the transition temperature T_c (derivation is shown in Appendix E). In Fig. 6(b) we plot the transition temperature T_c as a function of the deviation δn, for example, the parameters discussed previously. For $\delta n \sim 0.22$ we get $T_c \sim 0.2J_s$ ($\sim$1 nK). Thus, the ground state has a checkerboard density pattern due to the fermions in the s orbital and p-wave superfluid fermions in the p_z orbital at temperature below T_c. This can be considered an exotic supersolid. In contrast to the two-species models, s and p_z fermions are indistinguishable and, therefore, superfluid and CBW orders are not independent. This comes from the fact that onsite coupling U_{sp_z} includes the exchange term between fermions in the s and p_z orbitals. Such a term is not present in standard two-species models.

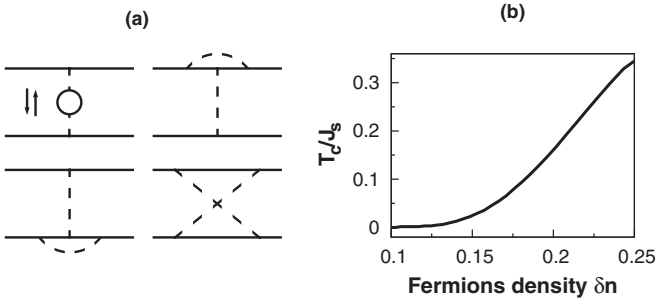

FIG. 6. (a) Diagrammatic representation of the second-order contributions in (10). The dashed lines denote interaction and the solid lines denote fermion propagator. (b) The p-wave superfluid transition temperature T_c as a function of density $n = 1/2 + \delta n$.

VI. CONCLUSIONS

In conclusion, we have derived a generalized Hubbard model for dipolar fermions in an optical lattice by taking into account higher orbitals. One important aspect of our findings is that the single-orbital Hubbard models of dipolar fermions as used in literature breaks down even for moderate dipole strengths and realistic trapping potentials. Furthermore, we have shown that the effect of these higher orbitals leads to interesting phenomena. Due to the strong interaction-dependent hopping terms in higher orbitals, these systems can be described by effective weakly interacting theories. For particular parameters, near $n \gtrsim 1/4$, we found a crossover to the one-dimensional physics resulting in simultaneous metallic and density wave properties. For $J_s \ll V_{ss}(\boldsymbol{e}_x)$, the s fermion checkerboard order is given by the configuration in Fig. 2(a). As J_s is increased there will be single-particle and dipole excitations at different regions of the $n = 1/4$ checkerboard crystal similar to the one considered in Ref. [26] for Wigner-Hubbard crystals due to Coloumb interaction. These excitations can induce interchain tunneling at different regions and the resulting model will be subject of future study. For other set of parameters, $n \gtrsim 1/2$, the system can be described by a weakly interacting Hubbard model with pseudospin originating from the lattice geometry. Using the KL theory, we found a transition to the chiral p-wave superfluidity due to the p_z fermions without destroying the checkerboard order created by the s fermions.

The parameters used here are experimentally realistic and for some parameters are even currently accessible. Nevertheless, let us note that to apply our theory for real experimental scenario one should take into account losses induced by reactivity of the molecules. In our paper we completely neglect this effect by assuming that the loss rates are much smaller than the considered tunneling processes. In fact, this is true even for highly reactive molecules like KRb. As reported in Ref. [27]

for a lattice depth of ~25 recoil energy ($\Omega \sim 5$) the loss rate in the p-orbital γ_{01} is of the order of $5 \times 10^2\ \mathrm{s}^{-1}$. In comparison, the interaction-induced interorbital tunneling rate $T^s_{p_z,p_{xz}}(-\boldsymbol{e}_x)$ is in the order of $5 \times 10^2\ \mathrm{s}^{-1}$ for $D = 8$ and $\Omega = 5$. It means that the ratio $\gamma / T^s_{p_z,p_{xz}}(-\boldsymbol{e}_x) \sim 1$, which can make the system stable with respect to such tunneling processes.

ACKNOWLEDGMENTS

This paper was supported by the EU STREP NAMEQUAM, IP AQUTE, ERC Grant QUAGATUA, Spanish MICINN (FIS2008-00784 and Consolider QOIT), AAII-Hubbard, and the Polish National Science Center Grant No. DEC-2011/01/D/ST2/02019. T.S. acknowledges support from the Foundation for Polish Science (KOLUMB Programme; KOL/7/2012) and hospitality from ICFO.

APPENDIX A: DERIVATION OF THE PARAMETERS U_{s,p_z}, $T^s_{p_z,p_z}$, AND $T^s_{p_z,p_{xz}}$

In this section we represent the onsite interaction term U_{s,p_z} and interaction-induced hopping terms $T^s_{p_z,p_z}$ and $T^s_{p_z,p_{xz}}$ in terms of the single-particle wave function $\mathcal{W}_{i\sigma}(\boldsymbol{r})$ in orbital σ localized on site $\boldsymbol{i}$. The orbital index $\sigma = \{pml\}$, denoting p, m, and l excitations in the x, y, and z directions, respectively. The s orbitals then can be written as $\mathcal{W}_{is}(\boldsymbol{r}) = w_{i_x0}(x)w_{i_y0}(y)\phi_0(z)$, where $w_{i_x0}(x), w_{i_y0}(y)$ are the lowest-band one-dimensional Wannier functions and $\phi_0(z)$ is the ground-state wave function of the harmonic oscillator in the z direction. Similarly, we can write $\mathcal{W}_{ip_z}(\boldsymbol{r}) = w_{i_x0}(x)w_{i_y0}(y)\phi_1(z)$ and $\mathcal{W}_{ip_{xz}}(\boldsymbol{r}) = w_{i_x1}(x)w_{i_y0}(y)\phi_1(z)$. Here $w_{i_x1}(x)$ is the Wannier functions in the first band and $\phi_1(z)$ is the first excited state of the harmonic oscillator in the z direction. For simplicity we took $\boldsymbol{j} = \boldsymbol{i} + \boldsymbol{e}_x$. From this we can write various parameters as

$$U_{s,p_z} = \int \left\{w_{i_x0}(x)w_{i_y0}(y)\right\}^2 \left\{w_{i_x0}(x')w_{i_y0}(y')\right\}^2 \times \Phi_{1,0}(z,z')\mathcal{V}(\boldsymbol{r}-\boldsymbol{r}')d\boldsymbol{r}d\boldsymbol{r}', \tag{A1a}$$

$$T^s_{p_z,p_z}(\boldsymbol{e}_x) = \int w_{j_x0}(x)w_{i_x0}(x)w^2_{i_x0}(x')\left\{w_{i_y0}(y)w_{i_y0}(y')\right\}^2 \times \Phi_{1,0}(z,z')\mathcal{V}(\boldsymbol{r}-\boldsymbol{r}')d\boldsymbol{r}d\boldsymbol{r}', \tag{A1b}$$

$$T^s_{p_z,p_{xz}}(\boldsymbol{e}_x) = \int w_{j_x1}(x)w_{i_x0}(x)w^2_{i_x0}(x')\left\{w_{i_y0}(y)w_{i_y0}(y')\right\}^2 \times \Phi_{1,0}(z,z')\mathcal{V}(\boldsymbol{r}-\boldsymbol{r}')d\boldsymbol{r}d\boldsymbol{r}', \tag{A1c}$$

$$\Phi_{1,0}(z,z') = \{\phi_1(z)\}^2\{\phi_0(z')\}^2 - \phi_1(z)\phi_0(z)\phi_1(z')\phi_0(z'). \tag{A1d}$$

The integrations over z,z' can be done analytically using convolution theorem in the momentum space. Consequently, in the momentum space we get

$$V(\boldsymbol{k}_\perp) = \mathcal{F}\left\{\int \Phi_{1,0}(z,z')\mathcal{V}(\boldsymbol{r}-\boldsymbol{r}')dzdz'\right\} = \frac{2\sqrt{2\pi}D}{l_z}\left[(kl_z)^2 - \sqrt{\frac{\pi}{2}}kl_z(1+(kl_z)^2)\mathrm{erfcx}\left(\frac{kl_z}{\sqrt{2}}\right)\right], \tag{A2}$$

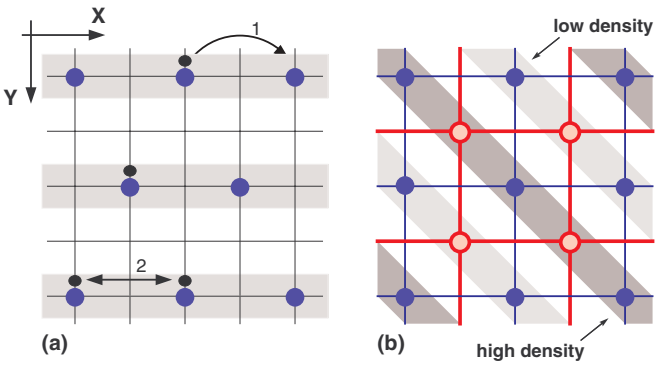

FIG. 7. (Color online) (a) Pictorial diagram for $n > 1/4$. The blue spheres denote s-orbital fermions and the smaller black spheres denote p_z orbital fermions. The s-orbital fermions constitute the underlying 1/4 checkerboard structure. The p_z fermions move with the effective tunneling $T^{\parallel}_{\mathrm{eff}}$ (arrow 1) only along the shaded regions. Interaction between neighboring p-band fermions is equal to $V_{p_z,p_z}(2\boldsymbol{e}_x)$ (arrow 2). (b) Density-wave structure at filling $\delta n = 1/4$. The dark and light shadings denote higher and lower density of the p_z fermions, respectively.

where $\mathcal{F}\{.\}$ denotes Fourier transform, $k = |\boldsymbol{k}_\perp| = \sqrt{k_x^2 + k_y^2}$, $l_z = (\hbar/m\Omega)^{1/2}$ is a natural harmonic oscillator length unit, and $\mathrm{erfcx}(x) = \exp(x^2)\mathrm{erfc}(x)$, where erfc(.) denotes complementary error function. It is important to note that $V(\boldsymbol{k}_\perp)$ is always negative for any $\boldsymbol{k}_\perp$. This explains the appearance of the attractive onsite interaction for any value of the confinement along the z direction.

APPENDIX B: LUTTINGER LIQUID DESCRIPTION FOR $n > 1/4$

As we explained in the main text, for filling $n > 1/4$ and parameters $V_0 = 8E_R$, $D = 10$, and $\hbar\Omega \sim 14E_R$, the ground-state structure is given by a 1/4 checkerboard structure formed by s fermions. The p_z fermions (with density $4n - 1$) move in the occupied sites along the **x** direction [Fig. 7(a)]. The resulting system can be thought as stacks of one-dimensional chains or stripes placed along **y** without interchain tunnelings. The effective Hamiltonian governing the p_z fermions can be written as (see the main text)

$$H_{1\mathrm{D}} = T^{\parallel}_{\mathrm{eff}} \sum_l \sum_{\langle ij\rangle} \hat{c}^\dagger_{l,i}\hat{c}_{l,j} + H_{\mathrm{intra}} + H_{\mathrm{inter}}, \tag{B1a}$$

$$H_{\mathrm{intra}} = \sum_l \sum_{i,j} V_{\mathrm{intra}}(i,j)\hat{c}^\dagger_{l,i}\hat{c}_{l,i}\hat{c}^\dagger_{l,j}\hat{c}_{l,j}, \tag{B1b}$$

$$H_{\mathrm{inter}} = \sum_{l,l'} \sum_{i,i'} V_{ll'}(i,i')\hat{c}^\dagger_{l,i}\hat{c}_{l,i}\hat{c}^\dagger_{l',i'}\hat{c}_{l',i'}. \tag{B1c}$$

The bosonized form of the intrachain Lagrangian reads

$$\mathcal{L}_{\mathrm{intra}} = u\int_{-\pi}^{\pi} \frac{dq_y}{2\pi}\frac{K_0}{2}\left\{\left[\frac{\partial\theta_{q_y}(x)}{\partial t}\right]^2 - \left[\frac{\partial\theta_{q_y}(x)}{\partial x}\right]^2\right\}, \tag{B2a}$$

where the Luttinger liquid parameter

$$K_0 = \left[\frac{2\pi T_{\rm eff}^{\parallel}\sin\tilde{k}_1 + \left[V_{p_z,p_z}(2\boldsymbol{e}_x)+\cdots\right](2-\cos 2\tilde{k}_1)}{2\pi T_{\rm eff}^{\parallel}\sin\tilde{k}_1 + \left[V_{p_z,p_z}(2\boldsymbol{e}_x)+\cdots\right]\cos 2\tilde{k}_1}\right]^{1/2}, \tag{B2b}$$

and the sound velocity

$$u^2 = \left(2\pi T_{\rm eff}^{\parallel}\sin\tilde{k}_1 + \left[V_{p_z,p_z}(2\boldsymbol{e}_x)+\cdots\right]\right)^2 - \left[V_{p_z,p_z}(2\boldsymbol{e}_x)+\cdots\right]^2(1-\cos 2\tilde{k}_1)^2. \tag{B2c}$$

We next include the bosonized form of the interchain Hamiltonian which results in the total Lagrangian $\mathcal{L}_{1D} = \mathcal{L} + \mathcal{L}_{\rm CDW}$, where

$$\mathcal{L} = u\int_{-\pi}^{\pi}\frac{dq_y}{2\pi}\frac{K(q_y)}{2}\left[\frac{1}{v(q_y)}\left(\frac{\partial\theta_{q_y}}{\partial t}\right)^2 - v(q_y)\left(\frac{\partial\theta_{q_y}}{\partial x}\right)^2\right]. \tag{B3}$$

Here the modified Luttinger parameter is given by

$$\frac{K(q_y)}{K_0} = \left[1+4\frac{\left[V_{p_z,p_z}(\boldsymbol{e}_x+2\boldsymbol{e}_y)+V_{p_z,p_z}(3\boldsymbol{e}_x+2\boldsymbol{e}_y)+\cdots\right]\cos(q_y)+\left[V_{p_z,p_z}(4\boldsymbol{e}_y)+\cdots\right]\cos(2q_y)}{2\pi T_{\rm eff}^{\parallel}\sin\tilde{k}_f+\left[V_{p_z,p_z}(2\boldsymbol{e}_x)+\cdots\right](2-\cos(2\tilde{k}_{f1}))}\right]^{1/2}, \tag{B4}$$

and sound velocity $v(q_y) = K(q_y)/K_0$. Interchain interactions induce an additional CDW perturbation, $\mathcal{L}_{\rm CDW} = \mathcal{L}_{\rm CDW,1} + \mathcal{L}_{\rm CDW,2} + \cdots$ with

$$\mathcal{L}_{\rm CDW,1} = \frac{1}{u}\sum_N V_{p_z,p_z}[(2N+1)\boldsymbol{e}_x + 2\boldsymbol{e}_y]\cos[(2N+1)\tilde{k}_1] \times \sum_l \cos[2\sqrt{\pi}(\theta_l - \theta_{l+1})], \tag{B5a}$$

$$\mathcal{L}_{\rm CDW,2} = \frac{1}{u}\sum_N V_{p_z,p_z}(2N\boldsymbol{e}_x + 4\boldsymbol{e}_y)\cos[(2N)\tilde{k}_1] \times \sum_l \cos[2\sqrt{\pi}(\theta_l - \theta_{l+2})]. \tag{B5b}$$

At half-filling, i.e., $\tilde{k}_1 = \pi/2$, we see that $\mathcal{L}_{\rm CDW,1} = 0$. It means that the charge-density wave instability is induced by the next-nearest neighbor interchain interaction. We checked that this interaction is much weaker than the tunneling $T_{\rm eff}^{\parallel}$. It means that the smectic-metal phase discussed in the paper will be stable to low-enough temperatures.

APPENDIX C: GROUND-STATE STRUCTURE OF *s*-ORBITAL FERMIONS AT $n = 1/2$

To look into the ground state of s-orbital fermions at $n = 1/2$, we express the average density $\langle\hat{n}_{i,s}\rangle = (1 + (-1)^{i_x+i_y}\delta)/2$, where δ is the order parameter. We also define the single-particle imaginary time Green functions $\mathcal{G}(\boldsymbol{i} - \boldsymbol{j},\tau) = \langle\mathcal{T}\hat{a}_{i,s}(\tau)\hat{a}^{\dagger}_{j,s}(0)\rangle$, where $\mathcal{T}$ denotes time ordering. By following the procedure described in Refs. [28,29] we find the following equations for $\mathcal{G}$ in the momentum space:

$$[\omega + \mu - 2V(1-\delta')]G_1(\boldsymbol{k},\omega) - \epsilon_{\boldsymbol{k}}G_2(\boldsymbol{k},\omega) = 1, \tag{C1a}$$

$$[\omega + \mu - 2V(1+\delta')]G_2(\boldsymbol{k},\omega) - \epsilon_{\boldsymbol{k}}G_1(\boldsymbol{k},\omega) = 0, \tag{C1b}$$

where the kinetic energy $\epsilon_{\boldsymbol{k}} = 2J_s(\cos k_x a + \cos k_y a)$, the effective potential $V = \sum_{\boldsymbol{i}\neq 0} V_{ss}(\boldsymbol{i})$, and $\delta' = \delta(\sum_{\boldsymbol{i}\in\rm odd} V_{ss}(\boldsymbol{i}) - \sum_{0\neq\boldsymbol{i}\in\rm even} V_{ss}(\boldsymbol{i}))/V$. In the position space $G_1(\boldsymbol{i})$ ($G_2(\boldsymbol{i})$) is equal to $\mathcal{G}(\boldsymbol{i})$ for $i_x + i_y$ even (odd). These mean-field equations for G_1 and G_2 are similar to the ones found for the extended Hubbard model, with a renormalized nearest-neighbor interaction and density imbalance [28,29]. Then, by solving equations (C1), we find that, in the strong coupling limit, $\delta = 1 - \frac{3J_s^2}{2V_{ss}^2(\boldsymbol{e}_x)}$ ($\delta \sim 0.98$ for $D = 8$ and $\hbar\Omega = 10E_R$). Thus, our assumption of a checkerboard lattice with alternative sites occupied is justified.

APPENDIX D: TRANSITION TEMPERATURE FOR STONER FERROMAGNETISM AND CHARGE-DENSITY WAVE INSTABILITY OF THE p_z FERMIONS FOR $n > 1/2$

In this section we discuss the appearance of Stoner ferromagnetism and CDW instability of the p_z fermions. To do this we transform to momentum space and introduce charge fluctuations $\rho_{\boldsymbol{q}} = \sum_{\boldsymbol{k},s} c^{\dagger}_{\boldsymbol{k}+\boldsymbol{q},s}c_{\boldsymbol{k},s}$ and spin fluctuations $S_{\boldsymbol{q}} = \sum_{\boldsymbol{k},s} s\, c^{\dagger}_{\boldsymbol{k}+\boldsymbol{q},s}c_{\boldsymbol{k},s}$ operators ($s \in \{\uparrow,\downarrow\}$). Subsequently, we rewrite Eq. (4) from the main text in the momentum space as

$$H_{\rm int} = \frac{1}{4}\sum_{\boldsymbol{q}}(2V_{\uparrow\uparrow}\eta_{\boldsymbol{q}} + V_{\uparrow\downarrow}\beta_{\boldsymbol{q}})\rho_{\boldsymbol{q}}\rho_{-\boldsymbol{q}} + \frac{1}{4}\sum_{\boldsymbol{q}}(2V_{\uparrow\uparrow}\eta_{\boldsymbol{q}} - V_{\uparrow\downarrow}\beta_{\boldsymbol{q}})S_{\boldsymbol{q}}S_{-\boldsymbol{q}}, \tag{D1}$$

where $\eta_{\boldsymbol{q}} = 2[\cos(q_x\widetilde{a}) + \cos(q_y\widetilde{a})]$ and $\beta_{\boldsymbol{q}} = 4[\cos(q_x\widetilde{a}/2)\cos(q_y\widetilde{a}/2)]$. The system with interactions described by (D1) can manifest three possible magnetic instabilities: CDW, spin-density wave (SDW), and ferromagnetic instability. At $\delta n = 1/4$ (each sublattice is half-filled with p_z-orbital fermions), as $\beta_{\boldsymbol{q}} = 0$ for nesting vector $\boldsymbol{q}\widetilde{a} = (\pm\pi,\pm\pi)$, interaction in the spin channel becomes repulsive and, therefore, SDW order is absent. In the spin channel, the onset of an Stoner ferromagnetism is given by the divergence of susceptibility with momentum $\boldsymbol{q} = (0,0)$. This condition can be written as $\lambda_{\rm st}\chi(0) = 1$, where $\lambda_{\rm st} = \frac{1}{2}[V_{\uparrow\downarrow}\beta_{\boldsymbol{0}} - 2V_{\uparrow\uparrow}\eta_{\boldsymbol{0}}]$, and the bare susceptibility $\chi(0) = \lim_{q\to 0}\int d\mathbf{p}\, Q_{\boldsymbol{q},\boldsymbol{p}}$ with $Q_{\boldsymbol{q},\boldsymbol{p}} = \frac{f(\epsilon_{\boldsymbol{p}}) - f(\epsilon_{\boldsymbol{p}-\boldsymbol{q}})}{\epsilon_{\boldsymbol{p}-\boldsymbol{q}} - \epsilon_{\boldsymbol{p}}}$. Here $f(\epsilon)$ is the Fermi distribution function and $\epsilon_{\boldsymbol{p}} = 2T_{\rm eff}^{\parallel}[\cos(q_x\widetilde{a}) + \cos(q_y\widetilde{a})]$ is the

dispersion relation. Consequently, in the limit of $T \to 0$, $\chi(0) = \int N(\epsilon)\, \partial_\epsilon f d\epsilon$ where the two-dimensional density of states,

$$N(\epsilon) = K[\sqrt{1-(\epsilon+\mu_p)^2/16T_{\rm eff}^{\parallel}}]/2\pi^2 T_{\rm eff}^{\parallel},$$

with $K(.)$ being an elliptic integral of first kind. Substituting the density of states we get $\chi(0) \approx N(T)$. As $\mu \to 0$, or density of p_z fermions are near $1/4$, due to the logarithmic divergence of K, the transition temperature for the Stoner ferromagnetism is given by

$$T_{\rm st} \approx 8T_{\rm eff}^{\parallel} \exp\left[-\frac{2\pi^2 T_{\rm eff}^{\parallel}}{\lambda_{\rm st}}\right].$$

The case $V_0 = 8E_R$, around $D \sim 8$, $\lambda_{\rm st}/2\pi^2 T_{\rm eff}^{\parallel} \sim 0.1$, corresponds to a very low Stoner temperature $T_{\rm st} \sim 10^{-4} T_{\rm eff}^{\parallel}$.

We next discuss the checkerboard charge-density wave structure due to the p_z fermions at $\delta n = 1/4$. Due to nesting, each fermionic component will be unstable towards CDW. In the density channel, the onset of an CDW is indicated by the divergence of susceptibility with momentum $\boldsymbol{q}\tilde{\boldsymbol{a}} = (\pi,\pi)$. The condition for p_z fermion CDW can be written as $\lambda_{\rm CDW}\chi(\pi,\pi) = -1$, where

$$\lambda_{\rm CDW} = \tfrac{1}{4}[2V_{\uparrow\uparrow}\eta_{(\pi,\pi)} + V_{\uparrow\downarrow}\beta_{(\pi,\pi)}] = -2V_{\uparrow\uparrow},$$

and the bare susceptibility

$$\chi(\pi,\pi) = \lim_{\boldsymbol{q}\to(\pi,\pi),\omega\to T} \int d\mathbf{p} \frac{f(\epsilon_{\boldsymbol{p}}) - f(\epsilon_{\boldsymbol{p}-\boldsymbol{q}})}{\omega - \epsilon_{\boldsymbol{p}-\boldsymbol{q}} + \epsilon_{\boldsymbol{p}}} \approx (\ln|8T_{\rm eff}^{\parallel}/T|)^2/2\pi^2 T_{\rm eff}^{\parallel}. \quad \text{(D2)}$$

Subsequently, the transition temperature to the CDW is given by $T_{\rm CDW} \approx 8T_{2,||}\exp(-\pi\sqrt{T_{\rm eff}^{\parallel}/V_{\uparrow\uparrow}})$. For example, when $V_0 = 8E_R$, $\hbar\Omega = 10E_R$, and $D = 8$ we find that $T_{\rm CDW} \approx 0.35J_s$ ($\sim$2 nK). One should note that due to the relative shift of sublattices the resulting density modulation in this phase looks like stripes rather than the standard checkerboard structure as shown in Fig. 7(b).

APPENDIX E: DERIVATION OF EFFECTIVE INTERACTION IN THE TRIPLET CHANNEL

In this section we derive the p-wave interaction from the Kohn-Luttinger effective interaction in terms of the scattering momentum $\boldsymbol{q} = \boldsymbol{k} - \boldsymbol{k}'$. For this purpose we rewrite Eq. (6) from the original paper

$$V_{{\rm eff}\,s,s}(\boldsymbol{q}) = V_{\uparrow\uparrow}\eta_{\boldsymbol{q}} - \sum_{\boldsymbol{p}}\big[\big(V_{\uparrow\uparrow}^2\,\eta_{\boldsymbol{q}}^2 + V_{\uparrow\downarrow}^2\,\beta_{\boldsymbol{q}}^2\big)Q_{\boldsymbol{q},\boldsymbol{p}} - 2V_{\uparrow\uparrow}^2\eta_{\boldsymbol{q}}\eta_{\boldsymbol{k}-\boldsymbol{p}}Q_{\boldsymbol{q},\boldsymbol{p}} - V_{\uparrow\uparrow}^2\eta_{\boldsymbol{k}'-\boldsymbol{p}}\eta_{\boldsymbol{k}-\boldsymbol{p}}Q_{\boldsymbol{k}+\boldsymbol{k}',\boldsymbol{p}}\big], \quad \text{(E1)}$$

where $Q_{\boldsymbol{p},\boldsymbol{q}} = \frac{f(\epsilon(\boldsymbol{p}))-f(\epsilon(\boldsymbol{p}-\boldsymbol{q}))}{\epsilon(\boldsymbol{p}-\boldsymbol{q})-\epsilon(\boldsymbol{p})}$ with $f(.)$ being the Fermi distribution function.

First, we put the expression of $\eta_{\boldsymbol{q}} = 2[\cos(q_x\tilde{a}) + \cos(q_y\tilde{a})]$ and $\beta_{\boldsymbol{q}} = 4[\cos(q_x\tilde{a}/2)\cos(q_y\tilde{a}/2)]$ back to (E1). As we are interested in p-wave interaction, after expanding (E1) in terms of the momenta k_x, k_x', k_y, k_y', we keep terms proportional to $\sin k_x\tilde{a}\sin k_x'\tilde{a} + \sin k_y\tilde{a}\sin k_y'\tilde{a}$. In this way we get

$$\begin{aligned}\{V_{\rm eff}(\boldsymbol{q})\} = \Big(&2V_{\uparrow\uparrow} - \sum_{\boldsymbol{p}} Q_{\boldsymbol{q},\boldsymbol{p}}[4(V_{\uparrow\downarrow})^2 - 8(V_{\uparrow\uparrow})^2 \\ &\times\{\cos(k_x\tilde{a} - p_x\tilde{a}) + \cos(k_y\tilde{a} - p_y\tilde{a})\}]\Big) \\ &\times(\sin k_x\tilde{a}\sin k_x'\tilde{a} + \sin k_y\tilde{a}\sin k_y'\tilde{a}) \\ &+ 4(V_{\uparrow\uparrow})^2\sum_{\boldsymbol{p}} Q_{\boldsymbol{q},\boldsymbol{p}}(\sin k_x\tilde{a}\sin k_x'\tilde{a}\sin^2 p_x\tilde{a} \\ &+ \sin k_y\tilde{a}\sin k_y'\tilde{a}\sin^2 p_y\tilde{a}), \end{aligned} \quad \text{(E2)}$$

where $\boldsymbol{q} = \boldsymbol{k} - \boldsymbol{k}'$. By converting sums to integrals in (E2) we have to compute terms of the form $\int d\,\boldsymbol{p}\,Q_{\boldsymbol{q},\boldsymbol{p}}$, $\int d\,\boldsymbol{p}\sin^2 p_x a_b\,Q_{\boldsymbol{q},\boldsymbol{p}}$, and $\int d\,\boldsymbol{p}\cos p_x a_b\,Q_{\boldsymbol{q},\boldsymbol{p}}$. In the limit of vanishing temperature $T \to 0$ we approximate all integrals $\int d\,\boldsymbol{p}G(\boldsymbol{p})\frac{f(\epsilon(\boldsymbol{p}))-f(\epsilon(\boldsymbol{p}-\boldsymbol{q}))}{\epsilon(\boldsymbol{p}-\boldsymbol{q})-\epsilon(\boldsymbol{p})} \approx \int N_{\rm eff}(\epsilon,\mu)\partial_\epsilon f d\epsilon$ for arbitrary function $G(\boldsymbol{p})$. The effective density of states reads $N_{\rm eff}(\epsilon,\mu) = \int d\boldsymbol{k}G(\boldsymbol{k})\delta(\epsilon - \epsilon_{\boldsymbol{k}})$. We see that the only first term inside the third bracket in (E2) is not dressed by $\cos(p_x\tilde{a})$ or $\sin(p_x\tilde{a})$. Hence, the effective density of states for this term contains Van Hove singularity. All other terms with in (E2), due to the dressing by $\cos(p_x\tilde{a})$ or $\sin(p_x\tilde{a})$, are analytic. For convenience, we reexpress $\{V_{\rm eff}(\boldsymbol{q})\}_- = -\lambda(T,\mu)[\sin(k_x\tilde{a})\sin(k_x'\tilde{a}) + \sin(k_y\tilde{a})\sin(k_y'\tilde{a})]$, where $\lambda(T,\mu) = 2V_{\uparrow\uparrow} + \frac{V_{\uparrow\uparrow}^2}{\pi T_{\rm eff}^{\parallel}}F_1(T,\mu) - \frac{V_{\uparrow\downarrow}^2}{\pi T_{\rm eff}^{\parallel}}F_2(T,\mu)$. The functions F_1 and F_2 are given by

$$F_1 = \frac{4}{\pi}F(1-(T+|\mu|)^2/(4T_{\rm eff}^{\parallel})^2), \quad \text{(E3a)}$$

$$F_2 = \frac{2}{\pi}K([1-(T+|\mu|)^2/(4T_{\rm eff}^{\parallel})^2), \quad \text{(E3b)}$$

where $F(x) = E(x) - (1-x)K(x)$ with $K(.)$ being the elliptic integral of the first kind and $E(.)$ is the elliptic integral of the second kind. Then we can write the BCS equation for the transition temperature T_c as [30]

$$V_p N_{\rm eff}(0,\mu)\log\left|\left(1-\left[\frac{\mu}{4T_{\rm eff}^{\parallel}}\right]^2\right)^{1/2}\frac{4T_{\rm eff}^{\parallel}}{T_c}\right| = 1, \quad \text{(E4)}$$

where the effective density of state is given by

$$N_{\rm eff}(\epsilon,\mu) = \sum_{\boldsymbol{k}}\delta(\epsilon+\mu-\epsilon_{\boldsymbol{k}})\sin^2(k_x a_b) \approx F[1-(\epsilon+|\mu|)^2/(4T_{\rm eff}^{\parallel})^2]/\pi^2 T_{\rm eff}^{\parallel}. \quad \text{(E5)}$$

As discussed in the main text, the ground state has a checkerboard density pattern due to the s fermions and p-wave superfluid p_z fermions at temperature below T_c. From previous section, we see that at $\delta n = 1/4$ (half-filled p_z fermions for the red and blue lattices), the transition temperatures for the p_z fermion CDW and p_z fermion superfluidity are similar. This will result in a competition or coexistence between both instabilities for the p_z orbital fermions. A detailed account of such scenario is beyond this scope of this paper.

[1] K. Ni *et al.*, Science **322**, 231 (2008).
[2] J. Deiglmayr *et al.*, Faraday Discuss. **142**, 335 (2009).
[3] M. Debatin *et al.*, Phys. Chem. Chem. Phys. **13**, 18926 (2011).
[4] J. W. Park *et al.*, Phys. Rev. A **85**, 051602(R) (2012).
[5] A. V. Gorshkov, S. R. Manmana, G. Chen, J. Ye, E. Demler, M. D. Lukin, and A. M. Rey, Phys. Rev. Lett. **107**, 115301 (2011).
[6] K. A. Kuns, A. M. Rey, and A. V. Gorshkov, Phys. Rev. A **84**, 063639 (2011).
[7] M. Lemeshko, R. V. Krems, and H. Weimer, Phys. Rev. Lett. **109**, 035301 (2012).
[8] K. Mikelsons and J. K. Freericks, Phys. Rev. A **83**, 043609 (2011).
[9] A.-L. Gadsbølle and G. M. Bruun, Phys. Rev. A **85**, 021604(R) (2012).
[10] S. G. Bhongale *et al.*, Phys. Rev. Lett. **108**, 145301 (2012).
[11] D.-S. Luehmann, O. Juergensen, and K. Sengstock, New J. Phys. **14**, 033021 (2012).
[12] A. Mering and M. Fleischhauer, Phys. Rev. A **83**, 063630 (2011).
[13] U. Bissbort, F. Deuretzbacher, and W. Hofstetter, arXiv: 1108.6047.
[14] S. Will *et al.*, Nature **465**, 197 (2010).
[15] O. Dutta *et al.*, New J. Phys. **13**, 023019 (2011).
[16] T. Sowiński, O. Dutta, P. Hauke, L. Tagliacozzo, and M. Lewenstein, Phys. Rev. Lett. **108**, 115301 (2012).
[17] S. Kotochigova and E. Tiesinga, Phys. Rev. A **73**, 041405 (2006).
[18] W. Kohn and J. M. Luttinger, Phys. Rev. Lett. **15**, 524 (1965).
[19] G. I. Watson, Physica A **246**, 253 (1997).
[20] T. Kennedy, Rev. Math. Phys. **6**, 901 (1994).
[21] B. Capogrosso-Sansone, C. Trefzger, M. Lewenstein, P. Zoller, and G. Pupillo, Phys. Rev. Lett. **104**, 125301 (2010).
[22] For our parameters, there can be localized excitations due to s-fermion tunneling with probability $\sim\exp(-0.3V_{s,s}(\boldsymbol{e}_x)/J_s) \approx 0.01$. Such excitations can couple two chains, but due to the small probability of such excitations we will neglect them.
[23] V. J. Emery, E. Fradkin, S. A. Kivelson, and T. C. Lubensky, Phys. Rev. Lett. **85**, 2160 (2000).
[24] A. Vishwanath and D. Carpentier, Phys. Rev. Lett. **86**, 676 (2001).
[25] R. Mukhopadhyay, C. L. Kane, and T. C. Lubensky, Phys. Rev. B **64**, 045120 (2001).
[26] S. Fratini and J. Merino, Phys. Rev. B **80**, 165110 (2009).
[27] A. Chotia, B. Neyenhuis, S. A. Moses, B. Yan, J. P. Covey, M. Foss-Feig, A. M. Rey, D. S. Jin, and J. Ye, Phys. Rev. Lett. **108**, 080405 (2012).
[28] M. Yu. Kagan, K. I. Kugel, and D. I. Khomskii, J. Eur. Theor. Phys. **93**, 415 (2001).
[29] D. I. Khomskii, Preprint of the P. N. Lebedev Physics Institute no. 105 (1969).
[30] R. Micnas, J. Ranninger, and S. Robaszkiewicz, Rev. Mod. Phys. **62**, 113 (1990).